water

MDPI

Article

Comparing the Adsorption Performance of Multiwalled Carbon Nanotubes Oxidized by Varying Degrees for Removal of Low Levels of Copper, Nickel and Chromium(VI) from Aqueous Solutions

Marko Šolić [1], Snežana Maletić [1,*], Marijana Kragulj Isakovski [1], Jasmina Nikić [1], Malcolm Watson [1], Zoltan Kónya [2,3] and Jelena Tričković [1]

1 Department of Chemistry, Biochemistry and Environmental Protection, Faculty of Sciences, University of Novi Sad, Trg Dositeja Obradovića 3, 21000 Novi Sad, Serbia; marko.solic@dh.uns.ac.rs (M.S.); marijana.kragulj@dh.uns.ac.rs (M.K.I.); jasmina.nikic@dh.uns.ac.rs (J.N.); malcolm.watson@dh.uns.ac.rs (M.W.); jelena.trickovic@dh.uns.ac.rs (J.T.)

2 Department of Applied and Environmental Chemistry, University of Szeged, Rerrich Béla tér 1, H-6720 Szeged, Hungary; konya@chem.u-szeged.hu

3 MTA-SZTE Reaction Kinetics and Surface Chemistry Research Group, Rerrich Béla tér 1, H-6720 Szeged, Hungary

* Correspondence: snezana.maletic@dh.uns.ac.rs; Tel.: +381-21-485-2727

Received: 31 January 2020; Accepted: 3 March 2020; Published: 6 March 2020

Abstract: Functionalized multiwalled carbon nanotubes (MWCNTs) have drawn wide attention in recent years as novel materials for the removal of heavy metals from the aquatic media. This paper investigates the effect that the functionalization (oxidation) process duration time (3 h or 6 h) has on the ability of MWCNTs to treat water contaminated with low levels of Cu(II), Ni(II) and Cr(VI) (initial concentrations 0.5–5 mg L^{-1}) and elucidates the adsorption mechanisms involved. Adsorbent characterization showed that the molar ratio of C and O in these materials was slightly lower for the oxMWCNT6h, due to the higher degree of oxidation, but the specific surface areas and mesopore volumes of these materials were very similar, suggesting that prolonging the functionalization duration had an insignificant effect on the physical characteristics of oxidized multiwalled carbon nanotubes (oxMWCNTs). Increasing the Ph of the solutions from Ph 2 to Ph 8 had a large positive impact on the removal of Cu(II) and Ni(II) by oxMWCNT, but reduced the adsorption of Cr(VI). However, the ionic strength of the solutions had far less pronounced effects. Coupled with the results of fitting the kinetics data to the Elowich and Weber–Morris models, we conclude that adsorption of Cu(II) and Ni(II) is largely driven by electrostatic interactions and surface complexation at the interface of the adsorbate/adsorbent system, whereas the slower adsorption of Cr(VI) on the oxMWCNTs investigated is controlled by an additional chemisorption step where Cr(VI) is reduced to Cr(III). Both oxMWCNT3h and oxMWCNT6h have high adsorption affinities for the heavy metals investigated, with adsorption capacities (expressed by the Freundlich coefficient K_F) ranging from 1.24 to 13.2 (mg g^{-1})/(mg l^{-1})^n, highlighting the great potential such adsorbents have in the removal of heavy metals from aqueous solutions.

Keywords: adsorption; heavy metals; carbon nanotubes; adsorption mechanism

1. Introduction

Heavy metals, as naturally occurring elements, can originate from both natural and anthropogenic sources. However, the increasing release of these pollutants in more toxic and mobile forms has made

anthropogenic sources a worldwide issue [1]. The main anthropogenic sources of heavy metals in the aquatic environment can be attributed to urbanization, industrialization (in particular the wastewater of modern chemical plants) and certain agricultural activities [1,2]. Metal processing and mining contribute to 48% of the total release of contaminants by the European industrial sector [3]. Heavy metals cannot undergo biodegradation processes and accumulate in the environment and living organisms at all levels of the food chain, making this group of pollutants even more noteworthy. A number of health problems may result from human exposure, intake and eventual buildup of non-essential (e.g., Cr(VI) and Ni) and even essential heavy metals (e.g., Cu) [2,4,5].

For this reason, the permissible concentrations of toxic elements in drinking water, surface waters and wastewaters before discharge to recipients, are set to very low levels. For example, the WHO provisional guideline values for Cu, Ni and Cr are 2 mg L^{-1}, 0.07 mg L^{-1} and 0.05 mg L^{-1}, respectively [6]. Emission levels for those metals in the most wastewater streams, according to the best available technologies, have been limited in the range of 0.01 to the 0.5 mg L^{-1} [7,8]. These concentrations are low, and thus, further treatment in order to comply with legislation is a difficult task. Conventional techniques such as chemical precipitation, coagulation and flocculation etc., are not efficient and are not able to remove low concentrations of target pollutants to permissible levels [2,9]. Techniques such as membrane filtration and ion exchange work well at low concentrations and achieve high efficacies, but suffer from disadvantages such as high operational cost and operational problems, etc. [1,10].

Adsorption can be an economically sustainable and viable solution for the removal of heavy metals from aqueous solutions. Adsorption has many advantages, such as simple operation, low cost, good Ph tolerance, and large industrial processing capacity [2,9,11,12]. However, there is still a need to develop and study new adsorbents, as many of the commonly applied adsorbent materials (activated carbons, zeolites, clay minerals, solid by-products of industrial processes and biosorbents) do not show satisfactory performance for the removal of heavy metals present in low concentrations [10]. Nanomaterials and especially carbon nanotubes (CNT) stand out as particularly promising materials to meet the requirements outlined above [4,10,11,13,14]. In order to achieve the desired level of efficiency for heavy metal removal, CNT functionalization has been widely investigated in recent years. The functionalization of CNT has already led to the development of new adsorbents for aqueous heavy metal treatments with state-of-the-art performance [10]. Even so, many review papers have recognized gaps in the current knowledge, whereby the majority of studies conducted concern the adsorption of very high concentrations of the heavy metals investigated, or do not explore the effects of preparation conditions on the functionalized nanomaterials (such as oxidation process duration, etc.) or the combined effects of different parameters on the adsorption process, or do not investigate the potential mechanism and chemistry involved in the heavy metals removal [1,4,10,11,13–16]. Oxidation of CNT is one of the simplest and therefore most economically viable functionalization techniques [10]. Regarding the removal of heavy metals such as Cu(II), Ni(II) and Cr(VI) by CNT, the literature data is very limited, with papers which deal with just one level of CNT oxidation and which investigate adsorption at high concentration levels above 10 mg L^{-1} [17–23].

The aim of this paper was therefore to investigate how the duration of the oxidation process of multiwalled carbon nanotubes (oxMWCNT3h or oxMWCNT6h) effects their use for the treatment of water contaminated with low levels of Cu(II), Ni(II) and Cr(VI), and to give insight into the adsorption mechanism of these metals on the oxidized MWCNTs. In order to achieve this goal, the synthesized adsorbents have been extensively characterized and the adsorption process was characterized by examining the contact time, the heavy metals concentration, and the Ph and ionic strength of the solutions.

2. Materials and Methods

2.1. Materials and Chemicals

Oxidized multiwalled carbon nanotubes (oxMWCNTs) were synthesized (by chemical vapour deposition) at the University of Szeged, according to the method described elsewhere [24].

Functionalization of MWCNTs was also carried out at the aforementioned institution under varying conditions to provide two different adsorbents for this study, following this procedure: (Step 1) 10 g of pristine MWCNTs was mixed with 1 L of cc. HNO_3 for 1 h by means of magnetic stirring, (Step 2) the obtained suspension was oxidized under reflux for 3 h (oxMWCNT3h) or 6 h (oxMWCNT6h), then (Step 3) rinsed with eionized water until neutral Ph was obtained. The oxMWCNTs selected for this study were then used as received. Stock solutions of Cu(II) and Ni(II) (100 mg L^{-1}) were prepared by diluting the appropriate metal standard solutions (1000 mg L^{-1}), while the Cr(VI) stock solution (100 mg L^{-1}) was obtained by dissolving $K_2Cr_2O_7$ in deionized water. The stock solutions were further diluted to the desired metals concentrations. All chemicals used in this research were analytical grade and were purchased from Merck Co. The experiments were performed using ultrapure deionized water (resistivity not less than 17.5 MΩ).

2.2. Adsorbents Characterisation

The specific surface areas, pore sizes, pore volumes and pore-size distributions of the investigated adsorbents were determined from nitrogen adsorption/desorption isotherms at 77 K, acquired by the AutosorbiQ Surface Area Analyzer (Quantachrome Instruments, USA). The specific surface areas were calculated using the multi-point Brunauer–Emmett–Teller (BET) method, while meso and micro pore volumes were obtained by the utilization of the desorption Barrett–Joyner–Halenda (BJH) isotherms and t-test method, respectively. Scanning electron microscopy (SEM) (TM3030, Hitachi High-Technologies, Japan) coupled with energy dispersive spectrometry (EDS) (Bruker Quantax 70 X-ray detector system, Bruker Nano, GmbH Germany) and transmission electron microscopy (TEM) (Philips CM10) were used to examine the materials morphological structures and surface elemental compositions. Identification of the functional groups present on the oxMWCNT3h and oxMWCNT6h was carried out by Fourier transform infrared (FTIR) spectrometry (Thermo-Nicolet Nexus 670 (USA) FTIR spectrometer), in the 4000–400 cm^{-1} range and in a diffuse reflection mode at a resolution of 4 cm^{-1}. The points of zero charge (pHpzc) of the adsorbents were obtained by adjusting the Ph value of 0.1 M $NaNO_3$ solutions in the range from 2 to 6, followed by measuring the Ph change of the $NaNO_3$/oxMWCNTs mixtures after 24 h of contact.

2.3. Adsorption Experiments

All adsorption studies were carried out in batch experiments conducted according to the following general procedure: (Step 1) 5 mg of oxMWCNT3h or oxMWCNT6h was weighed into 40 Ml glass vials, (Step 2) 30 Ml of background solution ($NaNO_3$) was added to each vial, (Step 3) oxMWCNT3h/$NaNO_3$ and oxMWCNT6h/$NaNO_3$ suspensions were subjected to 30 min of sonication (to enhance the dispersion of the adsorbents) (Ultrasons 1 litre bath), followed by stirring at 180 rpm (to pre-equilibrate oxMWCNTs and $NaNO_3$) for 24 h, (Step 4) stock solutions of Cu(II), Ni(II) or Cr(VI) were spiked to achieve desired concentrations of selected heavy metals, (Step 5) the Ph of adsorption systems was adjusted by adding 0.1 and/or 0.01 M NaOH or HNO_3, (Step 6) the adsorption systems were stirred for a certain period of time at 180 rpm and constant temperature of 298 K, (Step 7) the solid and liquid phases were separated by filtering the samples through 0.45 μm cellulose acetate membrane filters, (Step 8) the residual Cu(II), Ni(II) or Cr(VI) concentrations were determined using ICP-MS technique (Agilent Technologies 7700 Series ICP-MS). Method detection limits for the metals investigated were as follows: Cu(II): 0.001 mg L^{-1}, Ni(II): 0.001 mg L^{-1}, and Cr(VI): 0.001 mg L^{-1}.

The following deviations from this general procedure were made in order to investigate a variety of operational parameters: (1) influence of contact time—adsorption systems were stirred for various durations, ranging from 5 min to 24 h for Cu(II) and Ni(II), and in the case of Cr(VI), from 5 min to 168 h (Step 6); (2) influence of initial metal concentration—initial Cu(II), Ni(II) or Cr(VI) concentrations were varied between 0.5 and 5 mg L^{-1} (Step 4); (3) influence of Ph—initial sample Ph was adjusted to different values, ranging from 2 to 8 (Step 5); (4) influence of ionic strength—the $NaNO_3$ concentration in the background solutions was varied between 0.1 and 1 M (Step 2). Unless otherwise indicated,

operational parameters were: (1) contact time—24 h (Cu(II) and Ni(II)) and 96 h (Cr(VI)), (2) 1 mg L^{-1} initial metal concentration, (3) initial Ph = 5 (Cu(II) and Ni(II)) and Ph = 2.5 (Cr(VI)), (4) 0.1 M $NaNO_3$ ionic strength. The decision to investigate the effect of Ph and ionic strength in this work was made on the basis of the importance that the scientific literature assigns to these parameters.

In order to establish that the observed removals of heavy metals were a consequence of their adsorption on oxMWCNT3h and oxMWCNT6h, and not the result of some other processes (e.g., adsorption on glass vials walls, precipitation, etc.), triplicate blank experiments without the addition of the adsorbents were performed, according to the procedures given above. The levels of Cu(II), Ni(II) or Cr(VI) detected in these runs were used in all calculations as initial adsorbate concentrations. Experimental uncertainty, including instrumental errors, were determined using triplicates of the batch experiments and control samples in each adsorption series, with relative standard deviations falling mostly within ±5% of the reported values.

The adsorption capacities of oxMWCNT3h and oxMWCNT6h for the heavy metals investigated were calculated using mass balance Equation (1). Removal efficiencies of Cu(II), Ni(II) or Cr(VI) were determined by Equation (2).

$$q_t(or\ q_e) = \frac{(C_0 - C_t(or\ C_e))}{m} V \quad (1)$$

$$RE_t(or\ RE_e) = \frac{(C_0 - C_t(or\ C_e))}{C_0} \times 100 \quad (2)$$

where: q_t and q_e represent adsorption capacity per gram dry weight of the adsorbents at a specific time and at the state of equilibrium (mg g^{-1}); C_0, C_t and C_e are the initial, specific time and equilibrium adsorbate concentrations in the liquid phase (mg L^{-1}); V is the volume of the liquid phase (L); m is the dry weight of the adsorbent (g); RE_t and RE_e are the specific time and equilibrium adsorbate removal efficiencies (%).

2.4. Adsorption Kinetics and Isotherms Modelling

2.4.1. Adsorption Kinetics

In order to identify the adsorbate uptake rate, the rate-controlling step and to obtain insight into the possible mechanisms/reaction pathways of the investigated adsorption processes, four kinetic models (Lagergren pseudo-first order, pseudo-second order, Elovich and Weber–Morris (intra-particle diffusion)) were used to fit the experimental data.

The non-linear equations and parameters of the kinetic models tested, as well as information concerning their relationship to the potentially rate limiting adsorption steps, are provided in Table 1.

Table 1. Adsorption kinetics models.

Model	Model Equation	Model Parameters
Lagergren pseudo-first order [(a)]	$q_t = q_e\left(1 - e^{-k_1 t}\right)$	k_1—Lagergren pseudo-first order rate constant (h^{-1})
Pseudo-second order [(b)]	$q_t = \frac{{q_e}^2 k_2 t}{1+k_2 t q_e}$ $h = k_2 {q_e}^2$	k_2—pseudo-second order rate constant (g mg^{-1} h^{-1}) h—initial adsorption rate (mg g^{-1} h^{-1})
Elovich [(c)]	$q_t = \frac{1}{\beta}\ln(1 + \alpha\beta t)$	α—initial adsorption rate (g mg^{-1} h^{-2}) β—extent of surface coverage and the activation energy for chemisorption (g mg^{-1})
Weber–Morris (intra-particle diffusion) [(d)]	$q_t = k_3 t^{0.5}$	k_3—intra-particle diffusion rate constant (mg g $min^{0.5}$)

Note: Potential steps involved in heavy metal adsorption by porous adsorbents: (1) transport from bulk liquid phase to the external surface of the adsorbent; (2) passage through the liquid film attached to the solid surface; (3) interactions with the adsorbent surface (limiting step in reaction-based models [(a)], [(b)] and [(c)]; (4) diffusion into adsorbent internal sites (pores and interstitial channels) (limiting step in the diffusion-based [(d)] model) [25].

2.4.2. Adsorption Isotherms

In order to obtain data concerning the maximum adsorption capacity of the adsorbents, as well as to get a better understanding of the adsorption mechanisms, the Freundlich, Langmuir and Dubinin–Radushkevic (D–R) isotherm models were used to analyze the experimental equilibrium data.

The non-linear mathematical expressions, parameters and the most significant assumptions of the three applied models, along with the equations for the separation factor (also called the equilibrium parameter) and adsorption activation energy, which are essential features of the Langmuir and D–R isotherms, are given in Table 2.

Table 2. Adsorption isotherm models.

Model	Model Equation	Model Parameters
Freundlich [a]	$q_e = K_F {C_e}^n$	K_F—Freundlich constant indicating the adsorption capacity ((mg g^{-1}) (L mg^{-1})$^{1/n)}$ n—Freundlich exponent related to the energy distribution of adsorption sites (adsorption intensity) (dimensionless)
Langmuir [b]	$q_e = \frac{q_m K_L C_e}{1+K_L C_e}$ $R_L = \frac{1}{1+K_L C_0}$	q_m—maximum adsorption capacity (mg g^{-1}) K_L—Langmuir constant representing the energy of adsorption process (L mg^{-1}) R_L—Langmuir separation factor associated with adsorption favourability (dimensionless)
D-R[c] (∗)	$q_e = {q_d}^{-K_D RT\ ln(1+1/C_e)}$ $E_a = \frac{1}{\sqrt{2K_D}}$	q_d—maximum adsorption capacity (mg g^{-1}) K_D—D–R constant corresponding to the mean free energy of adsorption (mol2 K^{-1} J^{-2}) E_a—activation energy (kJ mol^{-1})

[a] An empirical equation describing multilayer adsorption onto energy-heterogeneous surfaces with interactions between adsorbed species. The stronger binding sites are occupied first and the binding strength decreases as site occupation increases. [b] A theoretical equation describing monolayer adsorption onto energy-homogenous surfaces with no lateral interaction and steric hindrance between the adsorbed molecules, even on adjacent sites. All binding sites are characterized by the same energy, which makes the binding strength identical throughout the adsorption process. [c] A semi-empirical equation describing adsorption with Gaussian energy distribution onto heterogeneous surfaces. It is usually applied to differentiate between physical and chemical adsorption of metal ions [26]. (*) R is the universal gas constant (8.314 J mol^{-1} K^{-1}).

3. Results and Discussion

3.1. Adsorbents Characterization

The TEM images of oxMWCNT3h and oxMWCNT6h are shown in Figure 1. The tubes are long and curved forming entangled oxMWCNTs networks. Note that the tubes have open ends as a result of the chemical functionalization (oxidation with cc. HNO_3) [17]. The opening up of the tubes has led to defects on the sidewalls of the nanotubes and has shortened their length. The inner tube diameters of oxMWCNT3h and oxMWCNT6h, ranged from 7–12 and 9–18 nm respectively, while the outer tube diameters of these materials were 15–24 and 7–32 nm [27].

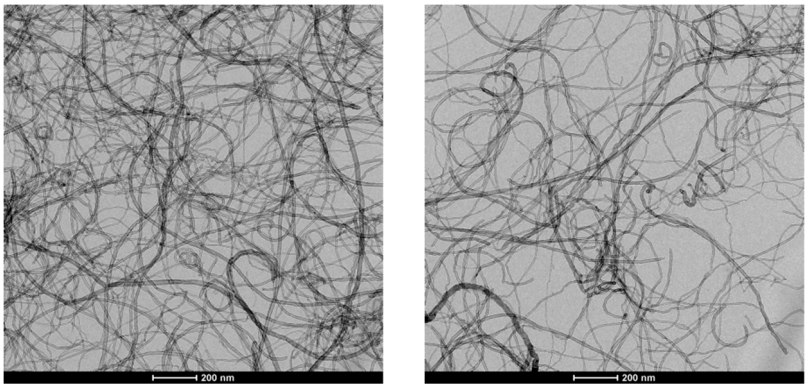

Figure 1. TEM images of: (**a**) oxMWCNT3h and (**b**) oxMWCNT6h.

Scanning electron microscopy was also used to investigate the surface morphology of oxMWCNT3h and oxMWCNT6h (Figure S1). It is evident that the surface of oxMWCNTs mainly consists of aggregated nanotubes. EDS analysis of oxMWCNT3h and oxMWCNT6h confirms that C and O are the dominant elements on the surface of these materials. The molar ratios of C and O in these materials were lower for oxMWCNT6h (11.32:1 compared to 9.32:1), as a consequence of the higher rate of oxidation. Traces of N originates from the HNO_3 which was used for functionalization of oxMWCNTs (Table S1).

The FTIR spectra of oxMWCNT3h and oxMWCNT6h are presented in Figure 2. Both spectra exhibit broad peaks at 3420 cm^{-1} which can be assigned to -OH stretching vibration of carboxylic and phenolic groups (-COOH and -COH). Absorption peaks at 2973 and 2923 cm^{-1} relate to the asymmetric and symmetric stretching vibrations of C–H originating from the surface of the tubes or from the sidewalls [20,28]. The peaks at 1630 and 1633 cm^{-1} can be attributed to bending vibration of –OH groups from physisorbed water molecules. The peaks at 1574, 1386, and 1396 cm^{-1}, observed in FTIR spectra of oxMWCNT3h, are associated with asymmetric and symmetric vibration of –COO groups [17,28]. Absorption peaks at 1046, 1086, and 1163 cm^{-1} in FTIR spectra of oxMWCNT3hare are associated with deformation vibrations of the –OH in alcohol, phenolic and carboxyl groups [20,21,28]. Generally, these oxygen-containing functional groups provide numerous adsorption sites and thus increase the adsorption capacity of the MWCNTs for metal ions [17,20].

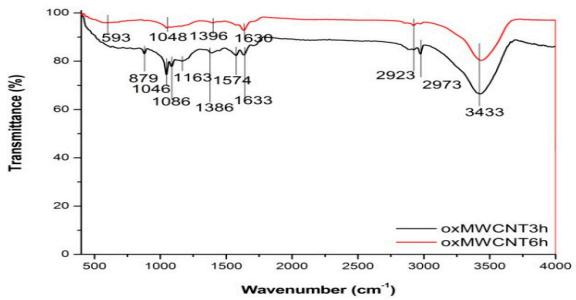

Figure 2. FTIR spectra of oxMWCNT3h and oxMWCNT6h.

The textural characteristics of oxMWCNT3h and oxMWCNT6h, including specific surface area, mesopore and micropore volumes and average pore size are shown in Table 3.

The specific surface areas of oxMWCNT3h and oxMWCNT6h, as well as the mesopore volume of these materials, were very similar, implying that the prolonged mixing time during functionalization has an insignificant effect on the physical characteristics of oxMWCNTs (Table 1). Moreover, the specific surface area of these materials is significantly higher than the specific surface area of MWCNTs which functionalized differently, using H_2O_2 and HNO_3 (in a ratio of 1:3 (v/v)) (196 m^2 g^{-1}) [17]. The point of zero charges of oxMWCNT3h and oxMWCNT6h are 3.2 and 3.4, respectively (Figure S2).

Table 3. Textural properties of oxMWCNT3h and oxMWCNT6h.

		oxMWCNT3h	oxMWCNT6h
Specific surface area	(m^2 g^{-1})	277	273
Mesopore volume (2–50 nm)	(cm^3 g^{-1})	1.95	1.65
Micropore volume (<2 nm)	(cm^3 g^{-1})	8×10^{-3}	1×10^{-3}
Average pore size	(nm)	14.2	12.2

3.2. Influence of Contact Time and Investigation of Adsorption Kinetics

3.2.1. Influence of Contact Time

The influence of contact time on the removal of Cu(II), Ni(II) and Cr(VI) by oxMWCNT3h and oxMWCNT6h, presented as q_t vs. t, is shown in Figure 3.

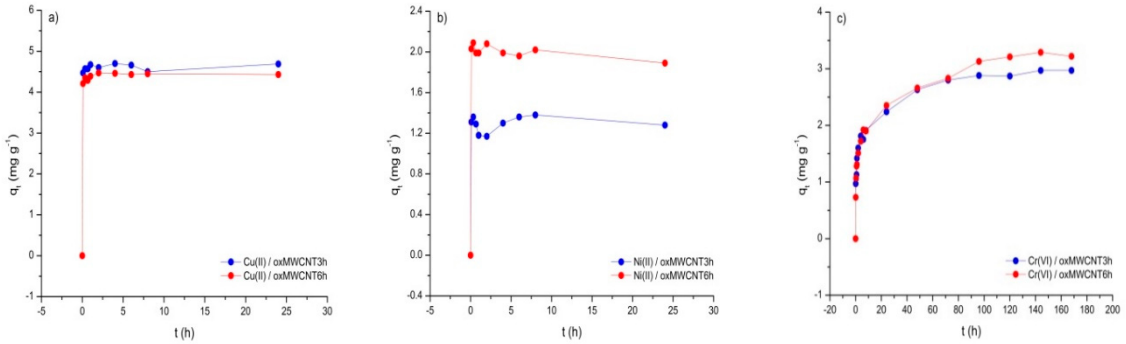

Figure 3. Adsorption of: (**a**) Cu(II), (**b**) Ni(II) and (**c**) Cr(VI) on oxMWCNT3h and oxMWCNT6h as a function of contact time (m = 5 mg, V = 30 mL (0.1 M $NaNO_3$), C_0 = 1 mg L^{-1}, pH = 5 ± 0.1 (Cu(II) and Ni(II)) and 2.5 ± 0.1 (Cr(VI)), t = 5 min-24 h (Cu(II) and Ni(II)) and 5 min-168 h (Cr(VI)), agitation speed = 180 rpm, T = 298 ± 2 K).

As can be seen in Figure 3, in the case of both investigated adsorbents, equilibrium for Cu(II) and Ni(II), was reached very quickly, in less than 20 min, indicating that the adsorption of these metals is predominantly controlled by the interactions taking place on the adsorbate/adsorbent surface. Throughout the entire studied duration, q_t (and RE_t) values remained very stable, averaging 4.60 mg g^{-1} (85.1%), 4.39 mg g^{-1} (93.0%), 1.29 mg g^{-1} (25.2%) and 2.00 mg g^{-1} (39.5%) for Cu(II) and Ni(II), respectively. Unlike in the case of Cu(II), the difference in the affinity of the studied oxMWCNTs for Ni(II) proved evident already in this type of adsorption experiments. Similar results have been obtained by other authors [23,25,29].

In contrast, the overall Cr(VI) adsorption rate for the two examined oxMWCNTs was much lower, with approximately 96 h required to reach equilibrium. Over the monitored period of time, the rate of Cr(VI) removal changed—during the first 8 h it was very high, and then slowly started to decline as the systems gradually approached a state of equilibrium. This behavior immediately suggests that Cr(VI) adsorption kinetics are controlled by more than one process of different physical origins (e.g., film diffusion, surface interactions and intra-particle diffusion), or that they are limited by the action of a single, but highly complex phenomenon (e.g., the presence of surface interactions or diffusion within pores of different dimensions) [30]. Clearly, the increased contact time was followed by an increase in q_t (and RE_t) values, resulting in equilibrium averages (q_e and RE_e) of 2.92 mg g^{-1} (47.8%) and 3.21 mg g^{-1} (58.5%) for oxMWCNT3h and oxMWCNT6h, respectively.

It is also important to note that the duration of the MWCNTs oxidation treatment did not affect the rate at which the equilibrium was reached in any of adsorption systems investigated (oxMWCNT3h = oxMWCNT3h; Cu(II) = Ni(II) > Cr(VI)). Based on the results obtained by these experiments, in order to ensure the feasibility of subsequent experiments, the time given to reach equilibrium in the studies

considering the influence of other selected operational parameters for Cu(II)/Ni(II) and Cr(VI) was set to be 24 and 96 h.

3.2.2. Adsorption Kinetics Modelling

Due to very rapid achievement of equilibrium, it was not possible to properly fit the Cu(II) and Ni(II) kinetics data to the kinetics models investigated. Further investigation of adsorption kinetics, utilizing the Lagergren pseudo-first order, pseudo-second order, Elovich and intra-particle diffusion models, was therefore only conducted in the case of Cr(VI).

Based on the R^2 values obtained by non-linear regression of the selected functions (Figure 4a,b), the best fit model was chosen. The calculated parameters of the corresponding equations are listed in Table 4. All the experimental data are in very good compliance with the Elovich model ($R^2 > 0.97$), which is generally valid for systems that are characterized by active chemical adsorption (without desorption of products), a process which includes the occurrence of valence forces, forming through sharing or exchanging of electrons between the adsorbate and the energetically heterogeneous surface of the adsorbent. The suitability of this model, additionally confirmed by the low χ^2 values (0.16 and 0.14; χ^2 determined by means of an χ^2 distribution table), also suggests that the observed decrease in Cr(VI) adsorption rate overtime on both oxMWCNTs is mainly due to the presence of different, complex surface interactions, the most important of which, in this respect, probably relates to very slow Cr(VI)/oxMWCNTs redox reactions (see Section 3.4.) [31–33]. When it comes to Elovich coefficients, it is noticeable that the β values are similar for the two applied adsorbents, whereas the α is more than twice as high for oxMWCNT3h (supported by comparable behavior in the pseudo-second order h values), therefore indicating a faster initial uptake for oxMWCNT3h.

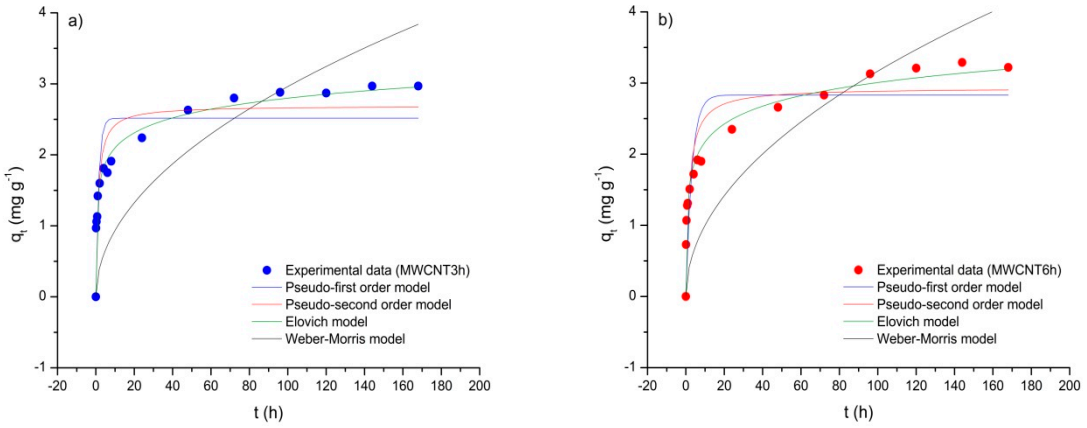

Figure 4. Non-linear regressions of kinetics data, obtained using Lagergren pseudo-first order, pseudo-second order, Elovich and intra-particle diffusion models for Cr(VI) adsorption on (**a**) oxMWCNT3h and (**b**) oxMWCNT6h.

It is important to note that in most of the scientific literature, the intra-particle diffusion model is linearly fitted [34]. According to this approach, intra-particle diffusion plays a significant role in controlling the kinetics only if q_t vs. $t^{0.5}$ produces a straight line passing through the origin of the plot (a zero intercept). Put differently, the deviation from linearity indicates that the adsorption rate is limited by some other process or processes. Furthermore, many authors state that the occurrence of multilinearity in Weber–Morris plots confirms the involvement of intra-particle diffusion in investigated adsorption mechanism, but again, not it the context of the rate-limiting step [35].

Table 4. Parameters of Lagergren pseudo-first order, pseudo-second order, Elovich and intra-particle diffusion models for the adsorption of Cr(VI) on oxMWCNT3h and oxMWCNT6h.

		oxFMWCNT3h	oxFMWCNT6h
Lagergren pseudo-first order	R^2	0.711	0.741
	k_1 (h^{-1})	0.697	0.322
	χ^2	2.051	3.750
	R^2	0.833	0.851
Pseudo-second order	R^2	0.833	0.851
	k_2 (g mg^{-1} h^{-1})	0.329	0.204
	h (g mg^{-1} h^{-1})	2.384	1.756
	χ^2	1.330	1.493
Elovich	R^2	0.981	0.984
	α (g mg^{-1} h^{-2})	30.600	14.562
	β (mg g^{-1} h^{-1})	3.295	2.760
	χ^2	0.160	0.142
Weber–Morris (non-linear)	$R_1{}^2$	0.066	0.342
	k_i(mg g^{-1} $h^{-0.5}$)	0.296	0.317
	χ^2	6.889	6.216
Weber–Morris (linear)	$R_1{}^2$	0.902	0.926
	k_i(mg g^{-1} $h^{-0.5}$)	0.155	0.183
	C_i (mg g^{-1})	1.270	1.195
	χ^2	13.003	11.490

The results obtained using this approach are shown in Figure 5a,b, with the corresponding parameters given in Table 4. As can be seen, both plots are multilinear (the red dashed lines) with the linear fit across the whole range of values yielding an intercept greater than zero (in Table 2 designated C_i). Therefore, as stated in the literature, it can be concluded that intra-particle diffusion, even if not the rate dominant factor, may be involved in the adsorption of Cr(VI) on oxMWCNT3h and oxMWCNT6h. Given the results shown in the Elowich and Weber–Morris models, these adsorption processes (in terms of rate and mechanism) are most likely controlled by complex surface interactions [20,36,37].

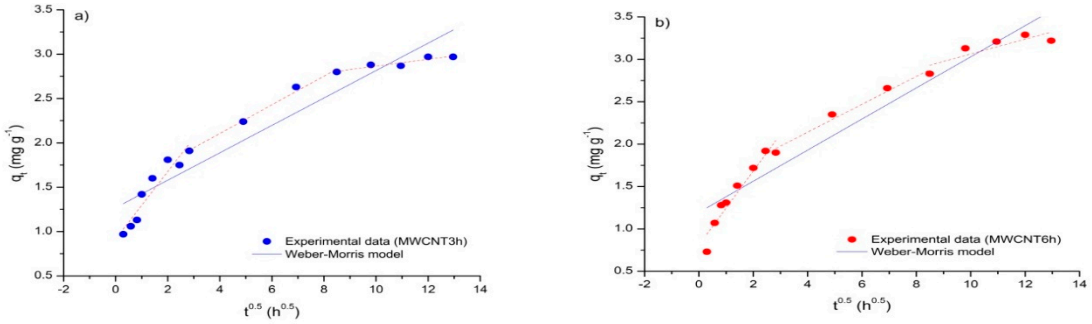

Figure 5. Linear regressions of experimental kinetics data, obtained using the intra-particle diffusion model for Cr(VI) adsorption on: (**a**) oxMWCNT3h and (**b**) oxMWCNT6h.

3.3. Modelling the Adsorption Isotherms (Influence of Initial Metal Concentration)

In order to describe the adsorption of Cu(II), Ni(II) and Cr(VI) on the oxMWCNTs investigated more precisely, the experimental data was analyzed using the Freundlich, Langmuir and D–R equations. The non-linear fitting curves resulting from these models are shown in Figure 6, while the parameters of these functions are given in Table 5.

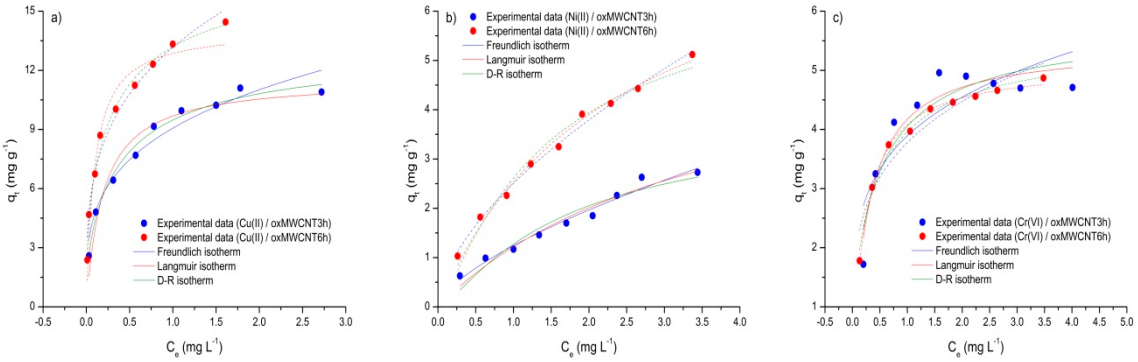

Figure 6. Non-linear regressions of experimental isotherms, obtained using Freundlcih, Langmuir and D–R models for: (**a**) Cu(II), (**b**) Ni(II) and (**c**) Cr(VI) adsorption on oxMWCNT3h and oxMWCNT6h (m = 5 mg, V = 30 mL (0.1 M $NaNO_3$), C_0 = 0.5–5 mg L^{-1},pH = 5 ± 0.1 (Cu(II) and Ni(II)) and 2.5 ± 0.1 (Cr(VI)), t = 24 h (Cu(II) and Ni(II)) and 96 h (Cr(VI)), agitation speed = 180 rpm, T = 298 ± 2 K).

Table 5. Parameters of Freundlich, Langmuir and D–R models for the adsorption of (**a**) Cu(II), (**b**) Ni(II) and (**c**) Cr(VI) on oxMWCNT3h and oxMWCNT6h.

		oxFMWCNT3h			oxFMWCNT6h		
		Cu(II)	**Ni(II)**	**Cr(VI)**	**Cu(II)**	**Ni(II)**	**Cr(VI)**
Freundlich	R^2	0.951	0.970	0.706	0.976	0.993	0.920
	K_F (*)	9.066	1.242	3.892	13.165	2.506	3.777
	n	0.281	0.662	0.225	0.286	0.598	0.244
	χ^2	0.474	0.062	0.858	0.695	0.031	0.217
Langmuir	R^2	0.946	0.954	0.920	0.946	0.988	0.994
	K_L (l mg^{-1})	5.129	0.273	3.331	10.459	0.428	3.996
	q_{max}(mg g^{-1})	11.567	5.691	5.422	14.086	8.455	5.100
	R_L	0.867–0.067	0.927–0.516	0.600–0.070	0.905–0.056	0.900–0.409	0.658–0.067
	χ^2	0.735	0.145	0.209	1.124	0.075	0.010
D–R	R^2	0.985	0.922	0.863	0.991	0.975	0.986
	q_d (mg g^{-1})	13.017	4.014	5.764	17.238	7.035	5.509
	K_d (mol^2 K^{-1} J^{-2})	1.846×10^{-4}	6.683×10^{-4}	2.051×10^{-4}	1.555×10^{-4}	5.765×10^{-4}	1.920×10^{-4}
	E_a (kJ mol^{-1})	52.050	27.353	49.376	56.702	29.450	51.027
	χ^2	0.112	0.252	0.369	0.212	0.157	0.037

(*) (mg g^{-1})/(mg l^{-1})^n.

High R^2 (> 0.91) and low χ^2 (< 1.12) values were obtained for all isotherms. The exception is the Freundlich and D–R isotherms of Cr(VI)/oxMWCNT3h, but even here the relatively low R^2 values (0.71 and 0.86) have corresponding acceptable χ^2 (0.86 and 0.37) values, suggesting that each of the three applied models is suitable for describing the adsorption of all the metals investigated on both oxMWCNT3h and oxMWCNT6h. The differences in the goodness of fit for Freundlich and Langmuir models are insignificant, so it is not possible to draw strong conclusions relating and number of adsorbate layers forming during the process.

Values of the Freundlich exponent n are less than 1 in each case, suggesting that all the processes can be characterized as favorable, with the adsorption of Cu(II) and Cr(VI) being good ($0.1 < n < 0.5$) and Ni(II) moderate ($0.5 < n < 1$) (Cu(II) ~ Cr(VI) > Ni(II)). This observation can be further substantiated by the R_L factors, which lie within the range 0 to 1 (adsorption is irreversible, favorable, linear or unfavorable, when $R_L = 0$, $0 < R_L < 1$, $R_L = 1$, $R_L > 1$, respectively). The generally high and significantly different K_F and K_L values obtained indicate the presence of selective adsorbents which have high affinities for the adsorption of the metals investigated.

Depending on how it is expressed, the adsorption capacity of oxMWCNT3h and oxMWCNT6h towards the selected metals exhibits the following trend: K_F (relative)—Cu(II) > Cr(VI) > Ni(II), q_m—Cu(II) > Ni(II) > Cr(VI), q_d—Cu(II) > Cr(VI) > Ni(II) (oxMWCNT3h) and Cu(II) > Ni(II) > Cr(VI) (oxMWCNT6h). Furthermore, the Cu(II) and Ni(II) removals were more pronounced for oxMWCNT6h, while the Cr(VI) uptake was slightly higher in the case of oxMWCNT3h (K_F, q_m, as well as q_d for the

adsorption of Cr(VI) on the applied adsorbents differs much less compared to the two other metals). These differences in the removal capacities of oxMWCNT3h and oxMWCNT6h (observed in the case of Cu(II) and Ni(II), and to a much lesser extent for Cr(VI)) are most likely due to the influence of the functionalization process length on the surface properties of the nanotubes (e.g., an increase in the quantity of various oxygen-containing groups with longer functionalization time; see Table S1), making them more suitable for the uptake of the divalent metals studied. Of the trends mentioned above, the experimental observations (q_e values) are most consistent with the values obtained by the Freundlich isotherm, so the assumptions behind this model can potentially be considered the most relevant for this study (see Table 2) [37,38].

Adsorption energies E_a, calculated using the D-R model, are greater than 16 kJ mol^{-1}, which implies that the formation of chemical bonds, as opposed to ion-exchange or non-specific physical interactions, dominantly controls all considered systems (adsorption is physical, ion-exchange or chemical type when 1 kJ mol^{-1} < E_a < 8 kJ mol^{-1}, 8 kJ mol^{-1} < E_a < 16 kJ mol^{-1}, E_a > 16 kJ mol^{-1}, respectively). This finding is consistent with the conclusions reached through non-linear modelling of the kinetics data [39].

A comprehensive overview of the capacity of other available adsorbents is given in the following papers [5,40,41]. As can be seen, oxMWCNT3h and oxMWCNT6h are, in most cases, characterized by a similar or lower adsorption capacity for Cu(II), Ni(II) and Cr(VI) compared to other materials. Considering the non-uniformity of the experimental conditions applied in different studies (e.g., C_0 range, initial pH value, m/V ratio, etc.), as well as the specificity of those under which this research was conducted (very low and narrow C_0 range and low m/V ratio) it is clear that the direct comparison of, for example, the q_{max} values obtained herein with the results of other authors, though possible, provides an unrealistic picture when it comes to efficiency of investigated oxMWCNTs.

3.4. Influence of pH

The solution pH acidity is the one matrix property with the highest potential to affect the adsorption of heavy metals. The removal of Cu(II), Ni(II) and Cr(VI) by oxMWCNT3h and oxMWCNT6h, as a function of pH, is illustrated in Figure 7.

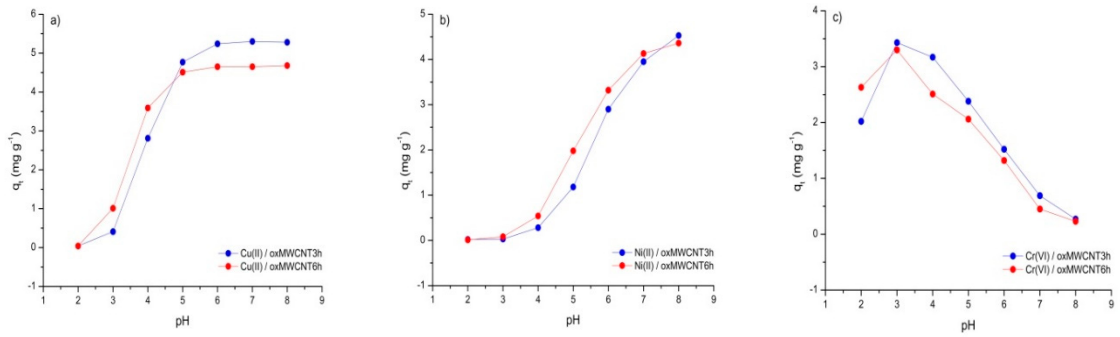

Figure 7. Adsorption of (**a**) Cu(II), (**b**) Ni(II) and (**c**) Cr(VI) on oxMWCNT3h and oxMWCNT6h as a function of pH (m = 5 mg, V = 30 mL (0.1 M $NaNO_3$), C_0 = 1 mg L^{-1}, pH = 2–8 ± 0.1, t = 24 h (Cu(II) and Ni(II)) and 96 h (Cr(VI)), agitation speed = 180 rpm, T = 298 ± 2 K).

As can be seen, pH plays an important role in the behavior of all studied adsorption systems. More specifically, Cu(II) uptake (q_e and RE_e) sharply increases as initial pH goes from 2 to 6 and then, as the liquid phase becomes more basic, maintains a constant high level (0.04 to 5.28 mg g^{-1} (0.70 to 99.4%) and 0.04 to 4.68 mg g^{-1} (0.92 to 99.3%)). oxMWCNTs capacity for Ni(II) rises throughout the entire pH range investigated (0.02 to 4.53 mg g^{-1} (0.40% to 82.2%), whereas the Cr(VI) systems demonstrated the best removals at pH = 3 (3.43 (59.9%) and 3.30 (64.1%)).

The influence of pH on adsorption can be explained by considering the effect this parameter has on the surface properties of the oxMWCNTs and the hydrolysis capacity of the selected metals. Depending

on the solution pH, oxygen-containing functional groups (e.g., -OH and -COOH), the presence of which was confirmed in the FTIR spectra, undergo protonation or deprotonation reactions, making the adsorbents net surface charge positive or negative depending upon where the solution pH lies in relation to the adsorbent pHpzc (Equations (3) and (4)).

$$Cx - OH + H^+ \leftrightarrow Cx - OH_2^+ \quad (3)$$

$$Cx - OH \leftrightarrow C_x - O^- + H^+ \quad (4)$$

where: Cx–OH, Cx–OH_2^+ and Cx–O^- are neutral, protonated and deprotonated sites on the oxMWCNTs surfaces (Cx is the adsorbent carbon surface, while –OH represents all the oxygen-containing functional groups).

Whether, and to what extent, certain heavy metals will interact with such adsorption centers, largely depends on the form/forms in which the metals are present in solution. Therefore, the Visual MINTEQ (version 3.1) software was used to predict the relative proportion of Cu(II), Ni(II) and Cr(VI) species present, with the results shown in Figure 8.

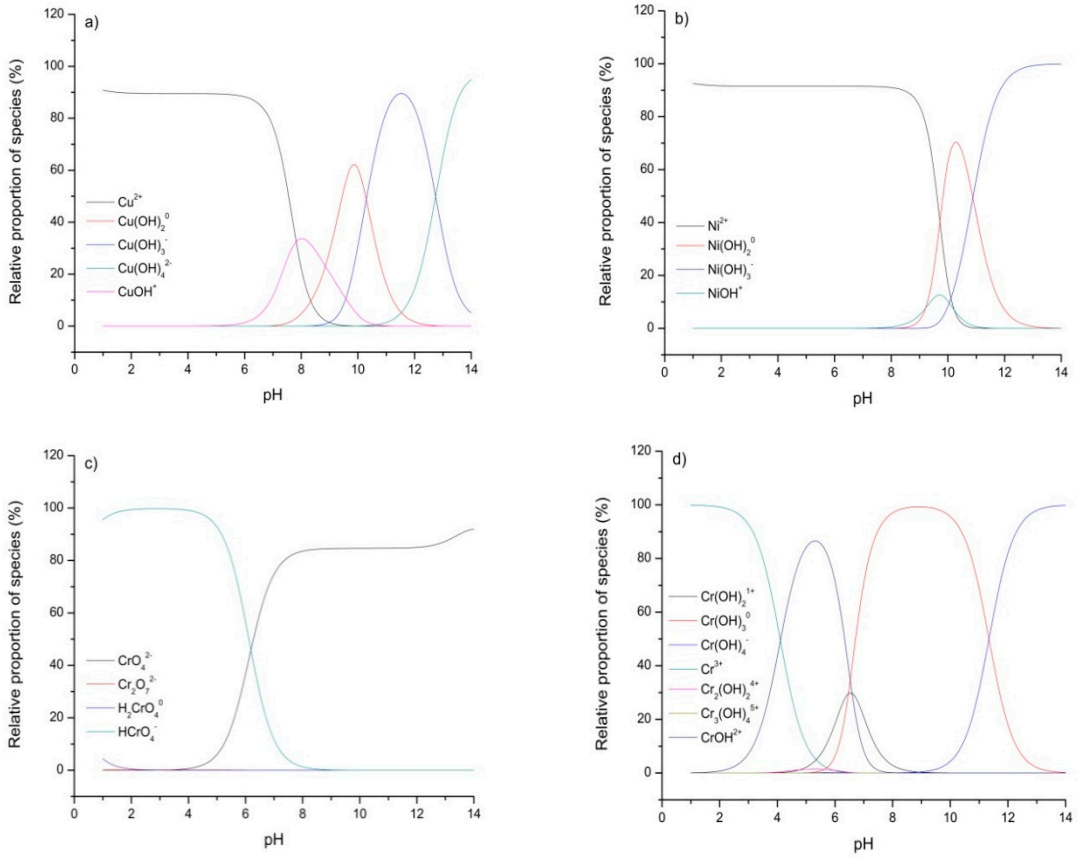

Figure 8. Relative proportion of: (**a**) Cu(II), (**b**) Ni(II), (**c**) Cr(VI) and (**d**) Cr(III) species as a function of pH (C_0 = 1 mg L^{-1}, ionic strength = 0.1 M $NaNO_3$, T = 298 K).

According to the plots in Figure 8a,b, at different pH values Cu(II) and Ni(II) exists as M^{2+}, $M(OH)^+$, $M(OH)_2{}^0$, $M(OH)_3{}^-$ and/or $M(OH)_4{}^{2-}$ (Cu(II) only) (M stands for metal). Hence, the low removal of Cu(II) and Ni(II) in strongly acidic media (pH < 4) can be partly attributed to the existence of competition between H^+ and M^{2+} aqua cations ($[(M(H_2O_6)]^{2+}$), the dominant form of these metals under given conditions, for the same oxygen-containing groups. The uptake of highly mobile H^+ ions is clearly more preferential than M^{2+} complex uptake, so most of oxMWCNTs surface sites become occupied and also positively charged (Equation (3)). This therefore hinders the adsorption of Cu(II)

and Ni(II) due to the unavailability of sites and electrostatic repulsion. In support of this, the pHpzc of the applied adsorbents was found to be very similar, ~3.2 and ~3.4, indicating that at low pH values oxMWCNT3h and oxMWCNT6h particles exhibit a net positive charge, which makes them incompatible to react with (adsorb) the divalent metals studied. The generally poor, but still evident removals of Cu(II) and Ni(II) in solutions of pH < 4 can be mainly attributed to their exchange with H^+ ions present on the oxMWCNTs surface (Equation (5)).

$$2Cx - OH_2^+ + M^{2+} \leftrightarrow [(Cx - OH)_2M]^+ + 2H^+ \quad (5)$$

When the pH goes up (H^+ concentration decreases), H^+/M^{2+} competition gradually begins to decline and certain acidic functional groups become more dissociated (Equation (4)), thus changing the net surface charge to negative (pH > pHpzc). In an environment like this, cationic metal ions, besides being electrostatically attracted by polarized, but not deprotonated centers (e.g., hydroxyl groups, pKa 9.5 to 13), easily form metal-ligand complexes with the now available, ionized nucleophilic sites, where the CNT oxygens act as electron-donating atoms (e.g., carboxyl (carboxylate) groups, pKa 1.7 to 4.7) (Equation (6) and only in the case of Cu(II) Equation (7)).

$$2C_x - CO^- + M^{2+} \leftrightarrow [(C_x - CO)_2M]^0 \quad (6)$$

$$C_x - CO^- + M(OH)^+ \leftrightarrow [C_x - COM(OH)]^0 \quad (7)$$

Note that beyond pH 7 Cu(II) begins to precipitate as relatively weakly soluble $Cu(OH)_2{}^0$ due to the more intense hydrolyzation. In contrast, Ni(II) remains stable over the entire tested pH range. Therefore, the removal of Cu(II) in more alkaline (pH 7 to 8) surroundings results from the simultaneous action of adsorption (Cu^{2+}, $Cu(OH)^+$) and also chemical deposition ($Cu(OH)_2{}^0$) [29,42,43].

The influence of pH on the extent of Cr(VI) uptake by oxMWCNT3h and oxMWCNT6h demonstrated an opposite effect to that described above. Namely, the capacity of oxMWCNTs for Cr(VI) at first increases, reaching a maximum at pH = 3, beyond which it begins to gradually decline. According to the speciation graph (Figure 8c), it is clear that in the highly acidic solutions (pH < 4) the most stable form of Cr(VI) is $HCrO_4{}^-$. These negatively charged oxyanions are readily electrostatically attracted and very likely chemically bonded (conclusion made on the basis of D–R isotherm model E_a values) to the oxMWCNTs surfaces (protonated and electrophilic centers), which are positive when pH < pHpzc, mainly asa consequence of the protonation of various weakly acidic and basic oxygen-containing functional groups (Equation (8)).

$$C_x - OH_2^+ + HCrO_4^- \leftrightarrow [C_x - OH_2CrO_4]^- + H^+ \quad (8)$$

The removal of Cr(VI) at low pH values can also take place through the occurrence of another ("indirect") mechanism, involving a three-step process: 1) reduction of $HCrO_4{}^-$ to Cr(III) by oxMWCNTs electron donors (various carboxyl and hydroxyl) groups. This reaction is maintained thanks to the high degree of Cr(VI) uptake at low pH; and the slow kinetics of this reaction are most likely responsible for the low Cr(VI) adsorption rate (Equation (9)), 2) release of Cr(III) species back into solution, 3) capturing Cr(III) aqua cations (mainly Cr^{3+}, speciation shown in Figure 8d) through the action of electrostatic attraction, chemisorption (deprotonated acidic sites) (Equation (10)) and ion exchange (protonated weakly acidic and basic sites) (Equation (11)). The $H^+/Cr(III)$ competition diminishes the effectiveness of this pathway, which is the reason why the total adsorption of Cr rises as pH goes up from pH 2 to pH 3.

$$3Cx - OH + HCrO_4^- + 4H^+ + 3e^- \leftrightarrow 3Cx - O^- + Cr^{3+} + 4H_2O \quad (9)$$

$$2C_x - CO^- + Cr^{3+} \leftrightarrow [(C_x - CO)_2Cr]^+ \quad (10)$$

$$2C_x - OH_2^+ + Cr^{3+} \leftrightarrow [(C_x - O)_2Cr]^{2+} + 2H^+ \quad (11)$$

It was not possible to confirm the presence of this mechanism via determination of the oxidation state of Cr (in solution or on the surfaces of oxMWCNT3h and oxMWCNT6h) after the adsorption process. However, the kinetic parameters, as well as the results of other authors who examined similar materials, clearly indicate its presence is likely [30].

At pH values greater than 3, deprotonation intensifies, the surface of the adsorbents becomes increasingly negative, and it becomes significantly more difficult for $HCrO_4^-$ to adsorb, due to electrostatic repulsion, according to Equation (8). This phenomenon is particularly pronounced in the case of higher charge number $Cr_2O_7^{2-}$ ions, the dominant form of Cr(VI) at pH > 6. Additionally, adsorption of oxyanions itself contributes to the negativity of oxMWCNTs surface, thus inhibiting the further removal of this metal. Finally, the existence of competition between excess OH^- and $HCrO_4^-/Cr_2O_7^{2-}$ for the same adsorption sites also has an adverse effect on the process studied [44].

3.5. Influence of Ionic Strength

The influence of the background electrolyte concentration on the degree of Cu(II), Ni(II) and Cr(VI) removal by oxMWCNT3h and oxMWCNT6h is illustrated in Figure 9. This is one of the potential controlling factors in any adsorption system.

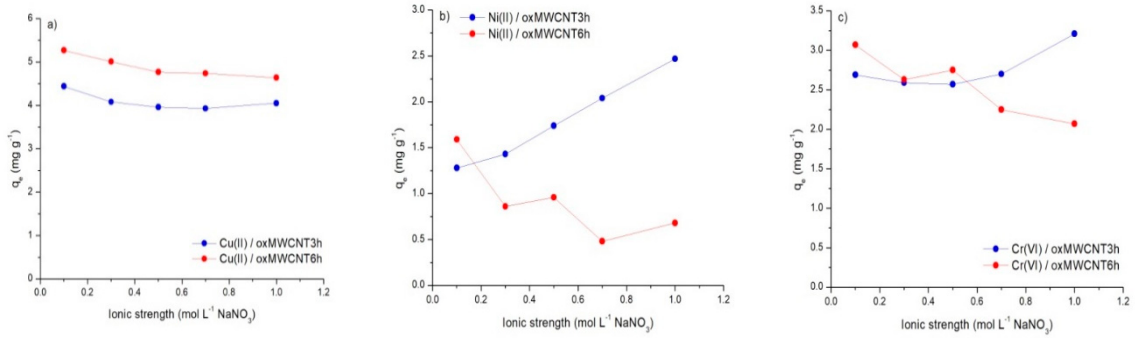

Figure 9. Adsorption of: (**a**) Cu(II), (**b**) Ni(II) and (**c**) Cr(VI) on oxMWCNT3h and oxMWCNT6h as a function of ionic strength (m = 5 mg, V = 30 mL (0.1–1 M $NaNO_3$), C_0 = 1 mg L^{-1}, pH = 5 ± 0.1 (Cu(II) and Ni(II)) and 2.5 ± 0.1 (Cr(VI)), t = 24 h (Cu(II) and Ni(II)) and 96 h (Cr(VI)), agitation speed = 180 rpm, T = 298 ± 2 K).

As can be seen, increasing the ionic strength from 0.1 to an extremely high level of 1 M $NaNO_3$, has a slight effect on the adsorption systems investigated, although it is considerably less than the effect of changing the solution pH. The observed variations in q_e (and RE_e) values are not completely consistent, even in the same metal/different adsorbent cases, and are located within the following limits: Cu(II)—3.93 to 4.44 mg g^{-1} (78.1% to 88.8%) and 4.64 to 5.27 mg g^{-1} (83.2% to 94.6%), Ni(II)—1.28 to 2.47 mg g^{-1} (25.4% to 48.5%) and 0.48 to 1.59 mg g^{-1} (8.5% to 28.1%), Cr(VI)—2.57 to 3.21 mg g^{-1} (48.0% to 60.0%) and 2.07 to 3.07 mg g^{-1} (34.7% to 51.2%). From the data reported above, it is clear that the greatest impact, be it positive or negative, depends on whether oxMWCNT3h or oxMWCNT6h is the adsorbent, in the case of adsorption of Ni(II).

Generally, when a solid charged surface is brought into contact with the liquid ionic medium, two layers of opposite polarity appear at the common boundary (interface) among the adjacent phases. Since the thickness of this electric double layer, as well as the interface potential, is determined by the background electrolyte concentration, the dominant types of interactions which take place on the related adsorbate/adsorbent exterior can be predicted.

According to the triple-layer (surface complexation) model, the uptake of Cu(II), Ni(II) and Cr(VI) associated with the oxMWCNTs surface, can occur in two different ways. The first of these involves the formation of inner-sphere complexes, that is partially or completely dehydrated metal ions directly and chemically specifically attached to adsorbent active sites. Such coordinatively bound species are

located in the so-called o-plane. The second one, designated as outer-sphere complexation, is realized through the occurrence of electrostatic attraction between fully solvated metal ions, placed in the β plane on a favorably charged surface. Bearing in mind that the outer-sphere ion-pairs are set in the same region as background electrolyte counterions, it is expected for them to be more susceptible to ionic strength variations than strongly adsorbed o-plane complexes [45].

Considering all of the above, the large increase in Na^+/NO_3^- concentration required to cause only narrow changes in q_e values, when taken into account together with the conclusions on the high pH-dependence of Cu(II), Ni(II) and Cr(VI) adsorption, clearly indicate that the inner-sphere surface complexation (chemisorption) can be designated as the dominant process in the removal of these heavy metals from solution. Outer-sphere complexes can therefore be ruled out, which means the role of background ions competition must be excluded from the explanation of the slight reduction in metals uptake at high Na^+/NO_3^- concentrations. Instead, this reduction is explained as follows: 1) a high ionic strength environment lowers the repulsive electrostatic energy of oxMWCNTs, which results in solid particles agglomeration (destabilization) and therefore a decrease in the number of available active sites; 2) introduction of Na^+/NO_3^- decreases the activity coefficients of Cu(II), Ni(II) and Cr(VI) ions, thus retarding their transfer to the adsorbent's surface. The positive influence of ionic strength, evident only when it comes to the Ni(II)/oxMWCNT3h system, may be attributed to diminishing of some repulsive electrostatic interactions, possibly as a consequence of developing the screening effect. This finding cannot be considered very reliable, especially due to the fact that Ni(II) behaves completely differently in the presence of oxMWCNT6h, which according to the characterization results, is fairly similar to oxMWCNT3h. The observations derived from these experiments do agree with and further confirm those made in the previous sections [19,30,46,47].

4. Conclusions

Taking into account all the results obtained, the following conclusions can be drawn:

The Cu(II) and Ni(II) adsorption systems reach a state of equilibrium very quickly, in less than 20 min. This indicates that the removal of these metals is mainly determined by the interactions occurring at the adsorbate/adsorbent surface. The Cr(VI) uptake rate, divided into two stages, is much slower, with 96 h required to achieve equilibrium. The duration of the MWCNTs oxidation treatment does not influence the kinetics of these adsorption processes (oxMWCNT3h = oxMWCNT3h; Cu(II) = Ni(II) > Cr(VI)).

The Cr(VI) adsorption kinetics are well described by the non-linear Elovich equation, which is valid for mechanisms dominated by chemisorption. According to the linearization of Weber–Morris plots, intra-particle diffusion may be involved, but is not a rate determining factor in Cr(VI) removal by oxMWCNT3h and oxMWCNT6h. Instead, the overall rate and mechanism of adsorption in this systems are controlled by complex surface interactions, the most important of which, in this respect, relates to very slow Cr(VI)/oxMWCNTs redox reactions.

The Freundlich, Langmuir and D–R isotherms are all in good compliance with the corresponding experimental data. Values of n, R_L and E_a indicate that the Cu(II), Ni(II) and Cr(VI) adsorption on the applied MWCNTs is favorable and chemically specific. The capacity of oxMWCNT3h and oxMWCNT6h for these metals expressed as K_F, the parameter most consistent with the non-fitted observations, follows the order: Cu(II) > Cr(VI) > Ni(II) (Cu(II) and Ni(II): oxMWCNT6h > oxMWCNT3h, Cr(VI): oxMWCNT3h ≥ oxMWCNT6h).

All the studied systems are strongly influenced by the solution pH. Specifically, Cu(II) uptake increases as the initial pH increases from 2 to 6, Ni(II) removal rises throughout the entire pH range investigated, while Cr(VI) is best adsorbed at pH = 3. Ionic strength has a far less pronounced effect on the behavior of the adsorption processes investigated. These findings further confirm that the most important factor in the complicated mechanism of Cu(II), Ni(II) and Cr(VI) adsorption on oxMWCNT3h and oxMWCNT6h is inner-sphere surface complexation (chemisorption) involving the coordination of metal ions with oxygen-containing functional groups.

Supplementary Materials: The following are available online at http://www.mdpi.com/2073-4441/12/3/723/s1, Figure S1: SEM images of: (a) oxMWCNT3h and (b) oxMWCNT6h., Figure S2: Points of zero charge of: (**a**) oxMWCNT3h and (**b**) oxMWCNT6h. Table S1: EDS analysis of oxMWCNT3h and oxMWCNT6h.

Author Contributions: Conceptualization, S.M. and M.Š.; methodology, S.M., M.Š. and M.K.I.; software, M.W.; validation, S.M., M.W. and M.K.I.; formal analysis, J.N.; investigation; resources, J.T. and Z.K.; data curation, M.Š.; writing—original draft preparation, M.Š.; writing—review and editing, S.M.; visualization, M.Š.; supervision, S.M.; project administration, J.T.; funding acquisition, J.T. All authors have read and agreed to the published version of the manuscript.

Funding: This research was funded by the Ministry of Education, Science and Technological Development of the Republic of Serbia (Project No. 451-03-68/2020-14/ 200125).

Acknowledgments: The authors gratefully acknowledge the support of the Ministry of Education, Science and Technological Development of the Republic of Serbia (Project No. 451-03-68/2020-14/ 200125).

Conflicts of Interest: The authors declare no conflict of interest.

References

1. Vareda, J.P.; Valente, A.J.M.; Durães, L. Assessment of heavy metal pollution from anthropogenic activities and remediation strategies: A review. *J. Environ. Manag.* **2019**, *246*, 101–118. [CrossRef] [PubMed]
2. Vardhan, K.H.; Kumar, P.S.; Panda, R.C. A review on heavy metal pollution, toxicity and remedial measures: Current trends and future perspectives. *J. Mol. Liq.* **2019**, *290*, 111197. [CrossRef]
3. Panagos, P.; Van Liedekerke, M.; Yigini, Y.; Montanarella, L. Contaminated Sites in Europe: Review of the Current Situation Based on Data Collected through a European Network. *Ecol. Indic.* **2013**, *24*, 439–450. [CrossRef]
4. Kumari, P.; Alam, M.; Siddiqi, W.A. Usage of nanoparticles as adsorbents for waste water treatment: An emerging trend. *Sustain. Mater. Technol.* **2019**, *22*, e00128. [CrossRef]
5. Yadav, V.B.; Gadi, R.; Kalra, S. Clay based nanocomposites for removal of heavy metals from water: A review. *J. Environ. Manag.* **2019**, *232*, 803–817. [CrossRef]
6. WHO. *Guidelines for Drinking-Water Quality*, 4th ed.; WHO: Geneva, Switzerland, 2012.
7. EU. European Commission Implementing Decision (EU) 2017/1442 of 31 July 2017 establishing best available techniques (BAT) conclusions, under Directive 2010/75/EU of the European Parliament and of the Council, for large combustion plants. *Off. J. Eur. Union* **2017**. Available online: http://www.legislation.gov.uk/eudn/2017/1442 (accessed on 5 March 2020).
8. EU. European Commission Implementing Decision (EU) 2016/1032 of 13 June 2016 establishing best available techniques (BAT) conclusions, under Directive 2010/75/EU of the European Parliament and of the Council, for the non-ferrous metals industries. *Off. J. Eur. Union* **2016**, 32–106. Available online: http://www.legislation.gov.uk/eudn/2016/1032 (accessed on 5 March 2020).
9. Nasir, A.M.; Goh, P.S.; Abdullah, M.S.; Ng, B.C.; Ismail, A.F. Adsorptive nanocomposite membranes for heavy metal remediation: Recent progresses and challenges. *Chemosphere* **2019**, *232*, 96–112. [CrossRef]
10. Xu, J.; Cao, Z.; Zhang, Y.; Yuan, Z.; Lou, Z.; Xu, X.; Wang, X. A review of functionalized carbon nanotubes and graphene for heavy metal adsorption from water: Preparation, application, and mechanism. *Chemosphere* **2018**, *195*, 351–364. [CrossRef]
11. Joseph, L.; Jun, B.-M.; Flora, J.R.V.; Park, C.M.; Yoon, Y. Removal of heavy metals from water sources in the developing world using low-cost materials: A review. *Chemosphere* **2019**, *229*, 142–159. [CrossRef]
12. Wang, L.; Wang, Y.; Ma, F.; Tankpa, V.; Bai, S.; Guo, X.; Wang, X. Mechanisms and reutilization of modified biochar used for removal of heavy metals from wastewater: A review. *Sci. Total Environ.* **2019**, *668*, 1298–1309. [CrossRef]
13. Fiyadh, S.S.; AlSaadi, M.A.; Jaafar, W.Z.; AlOmar, M.K.; Fayaed, S.S.; Mohd, N.S.; Hin, L.S.; El-Shafie, A. Review on heavy metal adsorption processes by carbon nanotubes. *J. Clean. Prod.* **2019**, *230*, 783–793. [CrossRef]
14. Gupta, N.K.; Choudhary, B.C.; Gupta, A.; Achary, S.N.; Sengupta, A. Graphene-based adsorbents for the separation of f-metals from waste solutions: A review. *J. Mol. Liq.* **2019**, *289*, 111121. [CrossRef]

15. Joseph, L.; Jun, B.-M.; Jang, M.; Park, C.M.; Muñoz-Senmache, J.C.; Hernández-Maldonado, A.J.; Heyden, A.; Yu, M.; Yoon, Y. Removal of contaminants of emerging concern by metal-organic framework nanoadsorbents: A review. *Chem. Eng. J.* **2019**, *369*, 928–946. [CrossRef]
16. Almeida, J.C.; Cardoso, C.E.D.; Tavares, D.S.; Freitas, R.; Trindade, T.; Vale, C.; Pereira, E. Chromium removal from contaminated waters using nanomaterials—A review. *TrAC Trends Anal. Chem.* **2019**, *118*, 277–291. [CrossRef]
17. Farghali, A.A.; Abdel Tawab, H.A.; Abdel Moaty, S.A.; Khaled, R. Functionalization of acidified multi-walled carbon nanotubes for removal of heavy metals in aqueous solutions. *J. Nanostruct. Chem.* **2017**, *7*, 101–111. [CrossRef]
18. Mobasherpour, I.; Salahi, E.; Ebrahimi, M. Removal of divalent nickel cations from aqueous solution by multi-walled carbon nano tubes: Equilibrium and kinetic processes. *Res. Chem. Intermed.* **2012**, *38*, 2205–2222. [CrossRef]
19. Ge, Y.; Li, Z.; Xiao, D.; Xiong, P.; Ye, N. Sulfonated multi-walled carbon nanotubes for the removal of copper (II) from aqueous solutions. *J. Ind. Eng. Chem.* **2014**, *20*, 1765–1771. [CrossRef]
20. Abdel-Ghani, N.T.; El-Chaghaby, G.A.; Helal, F.S. Individual and competitive adsorption of phenol and nickel onto multiwalled carbon nanotubes. *J. Adv. Res.* **2015**, *6*, 405–415. [CrossRef]
21. Zhao, X.H.; Jiao, F.P.; Yu, J.G.; Xi, Y.; Jiang, X.Y.; Chen, X.Q. Removal of Cu(II) from aqueous solutions by tartaric acid modified multi-walled carbon nanotubes. *Colloids Surfaces A Physicochem. Eng. Asp.* **2015**, *476*, 35–41. [CrossRef]
22. Kandah, M.I.; Meunier, J.L. Removal of nickel ions from water by multi-walled carbon nanotubes. *J. Hazard. Mater.* **2007**, *146*, 283–288. [CrossRef]
23. Kosa, S.A.; Al-Zhrani, G.; Abdel Salam, M. Removal of heavy metals from aqueous solutions by multi-walled carbon nanotubes modified with 8-hydroxyquinoline. *Chem. Eng. J.* **2012**, *181–182*, 159–168. [CrossRef]
24. Kanyó, T.; Kónya, Z.; Kukovecz, Á.; Berger, F.; Dékány, I.; Kiricsi, I. Quantitative characterization of hydrophilic-hydrophobic properties of MWNTs surfaces. *Langmuir* **2004**, *20*, 1656–1661. [CrossRef]
25. Abdel Salam, M.; Al-Zhrani, G.; Kosa, S.A. Removal of heavy metal ions from aqueous solution by multi-walled carbon nanotubes modified with 8-hydroxyquinoline: Kinetic study. *J. Ind. Eng. Chem.* **2014**, *20*, 572–580. [CrossRef]
26. Ayawei, N.; Ebelegi, A.N.; Wankasi, D. Modelling and Interpretation of Adsorption Isotherms. *J. Chem.* **2017**, *2017*, 3039817. [CrossRef]
27. Kragulj, M.; Tričković, J.; Dalmacija, B.; Kukovecz, Á.; Kónya, Z.; Molnar, J.; Rončević, S. Molecular interactions between organic compounds and functionally modified multiwalled carbon nanotubes. *Chem. Eng. J.* **2013**, *225*, 144–152. [CrossRef]
28. Wang, S.; Sun, H.; Ang, H.M.; Tadé, M.O. Adsorptive remediation of environmental pollutants using novel graphene-based nanomaterials. *Chem. Eng. J.* **2013**, *226*, 336–347. [CrossRef]
29. Yang, S.; Li, J.; Shao, D.; Hu, J.; Wang, X. Adsorption of Ni(II) on oxidized multi-walled carbon nanotubes: Effect of contact time, pH, foreign ions and PAA. *J. Hazard. Mater.* **2009**, *166*, 109–116. [CrossRef] [PubMed]
30. Hu, J.; Chen, C.; Zhu, X.; Wang, X. Removal of chromium from aqueous solution by using oxidized multiwalled carbon nanotubes. *J. Hazard. Mater.* **2009**, *162*, 1542–1550. [CrossRef]
31. Gholipour, M.; Hashemipour, H. Evaluation of multi-walled carbon nanotubes performance in adsorption and desorption of hexavalent chromium. *Chem. Ind. Chem. Eng. Q.* **2012**, *18*, 509–523. [CrossRef]
32. Can, M. Studies of the kinetics for rhodium adsorption onto gallic acid derived polymer: The application of nonlinear regression analysis. *Acta Phys. Pol. A* **2015**, *127*, 1308–1310. [CrossRef]
33. Lee, C.; Kim, S. Cr(VI) Adsorption to Magnetic Iron Oxide Nanoparticle-Multi-Walled Carbon Nanotube Adsorbents. *Water Environ. Res.* **2016**, *88*, 2111–2120. [CrossRef]
34. Tran, H.N.; You, S.J.; Hosseini-Bandegharaei, A.; Chao, H.P. Mistakes and inconsistencies regarding adsorption of contaminants from aqueous solutions: A critical review. *Water Res.* **2017**, *120*, 88–116. [CrossRef] [PubMed]
35. Jung, C.; Heo, J.; Han, J.; Her, N.; Lee, S.J.; Oh, J.; Ryu, J.; Yoon, Y. Hexavalent chromium removal by various adsorbents: Powdered activated carbon, chitosan, and single/multi-walled carbon nanotubes. *Sep. Purif. Technol.* **2013**, *106*, 63–71. [CrossRef]
36. Tofighy, M.A.; Mohammadi, T. Adsorption of divalent heavy metal ions from water using carbon nanotube sheets. *J. Hazard. Mater.* **2011**, *185*, 140–147. [CrossRef] [PubMed]

37. Zhang, X.; Huang, Q.; Liu, M.; Tian, J.; Zeng, G.; Li, Z.; Wang, K.; Zhang, Q.; Wan, Q.; Deng, F.; et al. Preparation of amine functionalized carbon nanotubes via a bioinspired strategy and their application in Cu^{2+} removal. *Appl. Surf. Sci.* **2015**, *343*, 19–27. [CrossRef]
38. Labied, R.; Benturki, O.; Eddine Hamitouche, A.Y.; Donnot, A. Adsorption of hexavalent chromium by activated carbon obtained from a waste lignocellulosic material (Ziziphus jujuba cores): Kinetic, equilibrium, and thermodynamic study. *Adsorpt. Sci. Technol.* **2018**, *36*, 1066–1099. [CrossRef]
39. Yu, F.; Wu, Y.; Ma, J.; Zhang, C. Adsorption of lead on multi-walled carbon nanotubes with different outer diameters and oxygen contents: Kinetics, isotherms and thermodynamics. *J. Environ. Sci. (China)* **2013**, *25*, 195–203. [CrossRef]
40. Burakov, A.E.; Galunin, E.V.; Burakova, I.V.; Kucherova, A.E.; Agarwal, S.; Tkachev, A.G.; Gupta, V.K. Adsorption of heavy metals on conventional and nanostructured materials for wastewater treatment purposes: A review. *Ecotoxicol. Environ. Saf.* **2018**, *148*, 702–712. [CrossRef]
41. Sarma, G.K.; Sen Gupta, S.; Bhattacharyya, K.G. Nanomaterials as versatile adsorbents for heavy metal ions in water: A review. *Environ. Sci. Pollut. Res.* **2019**, *26*, 6245–6278. [CrossRef]
42. Sun, X.; Liu, X.; Yang, B.; Xu, L.; Yu, S. Functionalized chrysotile nanotubes with mercapto groups and their Pb(II) and Cd(II) adsorption properties in aqueous solution. *J. Mol. Liq.* **2015**, *208*, 347–355. [CrossRef]
43. Xiao, D.L.; Li, H.; He, H.; Lin, R.; Zuo, P.L. Adsorption performance of carboxylated multi-wall carbon nanotube-Fe3O4 magnetic hybrids for Cu(II) in water. *Xinxing Tan Cailiao/New Carbon Mater.* **2014**, *29*, 15–25. [CrossRef]
44. Di Natale, F.; Lancia, A.; Molino, A.; Musmarra, D. Removal of chromium ions form aqueous solutions by adsorption on activated carbon and char. *J. Hazard. Mater.* **2007**, *145*, 381–390. [CrossRef] [PubMed]
45. Sheng, G.; Li, J.; Shao, D.; Hu, J.; Chen, C.; Chen, Y.; Wang, X. Adsorption of copper(II) on multiwalled carbon nanotubes in the absence and presence of humic or fulvic acids. *J. Hazard. Mater.* **2010**, *178*, 333–340. [CrossRef] [PubMed]
46. Chen, C.; Hu, J.; Shao, D.; Li, J.; Wang, X. Adsorption behavior of multiwall carbon nanotube/iron oxide magnetic composites for Ni(II) and Sr(II). *J. Hazard. Mater.* **2009**, *164*, 923–928. [CrossRef] [PubMed]
47. López-Ramón, V.; Moreno-Castilla, C.; Rivera-Utrilla, J.; Radovic, L.R. Ionic strength effects in aqueous phase adsorption of metal ions on activated carbons. *Carbon N. Y.* **2003**, *41*, 2020–2022. [CrossRef]